JACS ARTICLES

Published on Web 12/08/2010

Controllable Growth of Semiconductor Heterostructures Mediated by Bifunctional Ag_2S Nanocrystals as Catalyst or Source-Host

Guoxing Zhu and Zheng Xu*

State Key Laboratory of Coordination Chemistry, School of Chemistry and Chemical Engineering, Nanjing National Laboratory of Solid State Microstructure, Nanjing University, Nanjing 210093, China

Received October 10, 2010; E-mail: zhengxu@nju.edu.cn

Abstract: We demonstrate that Ag_2S nanocrystals are the bifunctional mediator for controllable growth of semiconductor heterostructures including more complicated multisegments heterostructures in solution-phase, which is a new type of nanomediator and quite different from the metal nanoparticle catalyst. The intrinsic high Ag^+ ion mobility makes Ag_2S nanocrystals not only exhibit excellent catalytic function for growth of metal sulfide heterostructures but also act as a source-host for growth of ternary semiconductor heterostructures, for example, Ag_2S-$AgInS_2$. The semiconductors grow epitaxially from or inward in Ag_2S nanocrystals forming single-crystalline heterostructures. Moreover, the method developed here also can construct multisegments heterostructures, for example, Ag_2S-CdS-ZnS, $AgInS_2$-Ag_2S-$AgInS_2$. The interfacial structure is still stable even if the lattice mismatch is quite large, which is a unique feature of this method.

Introduction

In the past few decades, great development has been achieved in the syntheses of various single component nanocrystals (NCs) with defined morphologies and dimensions. Further opportunities of nanoscience are afforded by the effective combination of two or more chemically distinct components in one single nanostructure with multifunctional or new properties induced by the heterointerfaces, which will undoubtedly lead to revolutionary new applications of nanomaterials in various areas, such as catalysis, photovoltaic devices, sensors, and so on.[1] The most recent developments of colloidal techniques, which benefit from modulating the solution/solid interfacial tension by means of organic surfactants, promote the fabrication of such elaborate heterostructure nanocrystals in solution,[2] especially for heterostructures with noncentrosymmetry. However, the synthesis of single-crystal semiconductor-based heterostructures is still a big challenge, while it is a prerequisite for exploring fundamental nanoscale semiconductor physics and offering technological devices with optimum characteristics because unintentional crystalline imperfections often lead to performance degradation or even premature failure of devices.[3]

To date, there are two types of solution routes in the literature for creating nano-objects with heterostructures: seeded growth[4] and catalyst-assisted growth.[5] In seeded growth, the second

(1) (a) Tada, H.; Mitsui, T.; Kiyonaga, T.; Akita, T.; Tanaka, K. *Nat. Mater.* **2006**, *5*, 782–786. (b) Mieszawska, A. J.; Jalilian, R.; Sumanasekera, G. U.; Zamborini, F. P. *Small* **2007**, *3*, 722–756. (c) Zhang, L. D.; Fang, X. S. *J. Nanosci. Nanotechnol.* **2008**, *8*, 149–201. (d) Khalavka, Y.; Sonnichsen, C. *Adv. Mater.* **2008**, *20*, 588–591. (e) Ong, P. L.; Levitsky, I. A. *Energies* **2010**, *3*, 313–334. (f) Amirav, L.; Alivisatos, A. P. *J. Phys. Chem. Lett.* **2010**, *1*, 1051–1054.

(2) (a) Cozzoli, P. D.; Pellegrino, T.; Manna, L. *Chem. Soc. Rev.* **2006**, *35*, 1195–1208. (b) Casavola, M.; Buonsanti, R.; Caputo, G.; Cozzoli, P. D. *Eur. J. Inorg. Chem.* **2008**, *6*, 837–838.

(3) Zhang, J. T.; Tang, Y.; Lee, K.; Ouyang, M. *Science* **2010**, *327*, 1634–1638.

(4) (a) Zeng, H.; Li, J.; Wang, Z. L.; Liu, J. P.; Sun, S. *Nano Lett.* **2004**, *4*, 187–190. (b) Gu, H.; Zheng, R.; Zhang, X.; Xu, B. *J. Am. Chem. Soc.* **2004**, *126*, 5664–5665. (c) Grebinski, J. W.; Hull, K. L.; Zhang, J.; Kosel, T. H.; Kuno, M. *Chem. Mater.* **2004**, *16*, 5260–5272. (d) Yu, H.; Chen, M.; Rice, P. M.; Wang, S. X.; White, R. L.; Sun, S. *Nano Lett.* **2005**, *5*, 379–382. (e) Kwon, K. W.; Shim, M. *J. Am. Chem. Soc.* **2005**, *127*, 10269–10275. (f) Buonsanti, R.; Grillo, V.; Carlino, E.; Giannini, C.; Curri, M. L.; Innocenti, C.; Sangregorio, C.; Achterhold, K.; Parak, F. G.; Agostiano, A.; Cozzoli, P. D. *J. Am. Chem. Soc.* **2006**, *128*, 16953–16970. (g) Talapin, D. V.; Nelson, J. H.; Shevchenko, E. V.; Aloni, S.; Sadtler, B.; Alivisatos, A. P. *Nano Lett.* **2007**, *7*, 2951–2959. (h) Kuo, C. H.; Hua, T. E.; Huang, M. H. *J. Am. Chem. Soc.* **2009**, *131*, 17871–17878. (i) Buonsanti, R.; Grillo, V.; Carlino, E.; Giannini, C.; Gozzo, F.; Garcia-Hernandez, M.; Garcia, M. A.; Cingolani, R.; Cozzoli, P. D. *J. Am. Chem. Soc.* **2010**, *132*, 2437–2464. (j) Chiu, W.; Khiew, P.; Cloke, M.; Isa, D.; Lim, H.; Tan, T.; Huang, N.; Radiman, S.; Abd-Shukor, R.; Hamid, M. A. A.; Chia, C. *J. Phys. Chem. C* **2010**, *114*, 8212–8218. (k) Acharya, K. P.; Hewa-Kasakarage, N. N.; Alabi, T. R.; Nemitz, I.; Khon, E.; Ullrich, B.; Anzenbacher, P.; Zamkov, M. *J. Phys. Chem. C* **2010**, *114*, 12496–12504.

(5) (a) Trentler, T. J.; Hickman, K. M.; Goel, S. C.; Viano, A. M.; Gibbons, P. C.; Buhro, W. E. *Science* **1995**, *270*, 1791–1794. (b) Markowitz, P. D.; Zach, M. P.; Gibbons, P. C.; Penner, R. M.; Buhro, W. E. *J. Am. Chem. Soc.* **2001**, *123*, 4502–4511. (c) Yu, H.; Li, J.; Loomis, R. A.; Wang, L. W.; Buhro, W. E. *Nat. Mater.* **2003**, *2*, 517–520. (d) Wang, F.; Dong, A.; Sun, J.; Tang, R.; Yu, H.; Buhro, W. E. *Inorg. Chem.* **2006**, *45*, 7511–7521. (e) Puthussery, J.; Lan, A.; Kosel, T. H.; Kuno, M. *ACS Nano* **2008**, *2*, 357–367. (f) Fanfair, D. D.; Korgel, B. A. *Cryst. Growth Des.* **2008**, *8*, 3246–3252. (g) Heitsch, A. T.; Hessel, C. M.; Akhavan, V. A.; Korgel, B. A. *Nano Lett.* **2009**, *9*, 3042–3047. (h) Chockla, A. M.; Korgel, B. A. *J. Mater. Chem.* **2009**, *19*, 996–1001. (i) Li, Z.; Cheng, L.; Sun, Q.; Zhu, Z.; Riley, M. J.; Aljada, M.; Cheng, Z.; Wang, X.; Hanson, G. R.; Qiao, S.; Smith, S. C.; Lu, G. Q. *Angew. Chem., Int. Ed.* **2010**, *49*, 2777–2781. (j) Aksomaityte, G.; Cheng, F.; Hector, A. L.; Hyde, J. R.; Levason, W.; Reid, G.; Smith, D. C.; Wilson, J. W.; Zhang, W. *Chem. Mater.* **2010**, *22*, 4246–4253.

10.1021/ja1090996

materials epitaxially grow on the suitable crystallographic facet offered by seeds, leading to heterostructure nanomaterials. Therefore, a proper lattice mismatch between the growing crystallographic facets of two different types of nanomaterials is required. Some cases of heterostructures fabricated through seeded growth have been reported, such as metal−metal,[6] metal−semiconductor,[7] and semiconductor−semiconductor[8] systems.

Although the principle of seed-assistant growth is easy to understand, the fabrication of single-crystal heterostructures is highly difficult in experiment, because the self-nucleation of the second material is difficult to be completely avoided. And also, accurately controlling the surface states of seed, which is suitable for epitaxial growth of the second materials, is also difficult. The try and error method was adopted to search the optimum experiment parameters such as temperature, concentration of the precursors, surfactants (including the types, concentrations, and often rigorous combination of two or more different ones), feeding way, and so on, which is tremendously trivial and tedious.[2,9]

In catalyst-assisted growth, including solution−liquid−solid (SLS)[5d,10] and "supercritical fluid−liquid−solid" (SLFS) methods,[5d,10b] a metal or alloy with a low melting point is used as a catalyst for growing nanowires. This route works at a relatively elevated temperature, at which the metal nanoparticle catalyst shows liquid or quasi-liquid owing to its smaller size and low melt points, dissociates the dissolved precursor, and absorbs the species that can be dissolved in the catalyst. The aim materials grow from the resulting supersaturation catalyst at the liquid−solid interface in a manner that minimizes the interface energy. In such a proposed model, the liquid catalyst acts as a medium for transporting species from the solution phase to the solid product. There are several prerequisites for the catalyst:[11a] (1) the melting point must be below the reaction temperature causing the catalyst particles to be liquid or quasi-liquid; (2) the solubility of the aim materials in the catalyst should be limited; (3) there is no possibility to form a solid solution between catalyst and aim materials. To date, the catalyst nanoparticles that meet the above prerequisites are exclusively chosen from metals such as Al_xGa_{1-x} alloys,[5b] In,[5c] Bi,[5f] Au,[5g,h] or Au@Bi core−shell nanoparticles,[5e] which is more suitable for preparing semiconductor nanowires or heterostructures of metal-semiconductor. Compared with the catalytic growth of semiconductor nanowires, the catalytic growth of 1D semiconductor-semiconductor nanoheterostructure is quite rare. Recently, the catalytic fabrication of $Cu_2S-In_2S_3$ heterostructure by using $Cu_{1.94}S$ NCs as a catalyst has been reported, in which copper sulfide underwent transformations in both crystalline structure and chemical composition (from monoclinic djurleite to hexagonal chalcocite) during the formation of the heterostructure,[11a] whereas the same heterostructures were also prepared by using Cu_2S NCs as seeds in solution.[11b] More interestingly, Cu_2S-$CuInS_2$ heterostructure was fabricated in the same reaction system as Hyeon's including the same precursors through a Cu_2S seed mediated method.[12] From these results, we learned that copper sulfide can act as both seed or catalyst in a similar reaction system, and In^{3+} does not dissolve in hexagonal phase Cu_2S but in monoclinic phase $Cu_{1.94}S$. More interesting, even though In^{3+} can dissolve in $Cu_{1.94}S$, no $CuInS_2$ species are formed in the copper sulfide. The origin for these is not clear at the present time and further studies are urgently needed. Also, understanding these not only can allow precise control over the fabrication of semiconductor−semiconductor heterostructures, especially for $I-III-VI_2$ ternary semiconductor compounds such as $AgInS_2$,[13] $CuInS_2$,[13,14] $CuInSe_2$,[14a] $CuGaS_2$,[15] due to their adjustable band gap energies and having promise for photovoltaic applications,[14a] but also can promote the exploitation of

(6) (a) Chen, J.; Wiley, B.; McLellan, J.; Xiong, Y.; Li, Z. Y.; Xia, Y. *Nano Lett.* **2005**, *5*, 2058–2062. (b) Pellegrino, T.; Fiore, A.; Carlino, E.; Giannini, C.; Cozzoli, P. D.; Ciccarella, G.; Respaud, M.; Palmirotta, L.; Cingolani, R.; Manna, L. *J. Am. Chem. Soc.* **2006**, *128*, 6690–6698. (c) Xiang, Y.; Wu, X.; Liu, D.; Jiang, X.; Chu, W.; Li, Z.; Ma, Y.; Zhou, W.; Xie, S. *Nano Lett.* **2006**, *6*, 2290–2294. (d) Habas, S.; Lee, H.; Radmilovic, V.; Somorjai, G.; Yang, P. *Nat. Mater.* **2007**, *6*, 692–697. (e) Ferrer, D.; Torres-Castro, A.; Gao, X.; Sepulveda-Guzman, S.; Ortiz-Mendez, U.; Jose-Yacaman, M. *Nano Lett.* **2007**, *7*, 1701–1705. (f) Wetz, F.; Soulantica, K.; Falqui, A.; Respaud, M.; Snoeck, E.; Chaudret, B. *Angew. Chem., Int. Ed.* **2007**, *46*, 7079–7081. (g) Fan, F. R.; Liu, D. Y.; Wu, Y. F.; Duan, S.; Xie, Z. X.; Jiang, Z. Y.; Tian, Z. Q. *J. Am. Chem. Soc.* **2008**, *130*, 6949–6951. (h) Lee, Y. W.; Kim, M.; Kim, Z. H.; Han, S. W. *J. Am. Chem. Soc.* **2009**, *131*, 17036–17037.

(7) (a) Mokari, T.; Rothenberg, E.; Popov, I.; Costi, R.; Banin, U. *Science* **2004**, *304*, 1787–1790. (b) Pacholski, C.; Kornowski, A.; Weller, H. *Angew. Chem., Int. Ed.* **2004**, *43*, 4774–4777. (c) Mokari, T.; Sztrum, C. G.; Salant, A.; Rabani, E.; Banin, U. *Nat. Mater.* **2005**, *4*, 855–863. (d) Carbone, L.; Kudera, S.; Giannini, C.; Ciccarella, G.; Cingolani, R.; Cozzoli, P. D.; Manna, L. *J. Mater. Chem.* **2006**, *16*, 3952–3956. (e) Dukovic, G.; Merkle, M. G.; Nelson, J. H.; Hughes, S. M.; Alivisatos, A. P. *Adv. Mater.* **2008**, *20*, 4306–4311. (f) Habas, S. E.; Yang, P.; Mokari, T. *J. Am. Chem. Soc.* **2008**, *130*, 3294–3295. (g) Lee, J. S.; Bodnarchuk, M. I.; Shevchenko, E. V.; Talapin, D. V. *J. Am. Chem. Soc.* **2010**, *132*, 6382–6391.

(8) (a) Talapin, D. V.; Koeppe, R.; Gotzinger, S.; Kornowski, A.; Lupton, J. M.; Rogach, A. L.; Benson, O.; Feldmann, J.; Weller, H. *Nano Lett.* **2003**, *3*, 1677–1681. (b) Teranishi, T.; Inoue, Y.; Nakaya, M.; Oumi, Y.; Sano, T. *J. Am. Chem. Soc.* **2004**, *126*, 9914–9915. (c) Shieh, F.; Saunders, A. E.; Korgel, B. A. *J. Phys. Chem. B* **2005**, *109*, 8538–8542. (d) Kudera, S.; Carbone, L.; Casula, M. F.; Cingolani, R.; Falqui, A.; Snoeck, E.; Parak, W. J.; Manna, L. *Nano Lett.* **2005**, *5*, 445–449. (e) Halpert, J. E.; Porter, V. J.; Zimmer, J. P.; Bawendi, M. G. *J. Am. Chem. Soc.* **2006**, *128*, 12590–12591. (f) Xie, R.; Kolb, U.; Basche, T. *Small* **2006**, *2*, 1454–1457. (g) Dong, A.; Wang, F.; Daulton, T. L.; Buhro, W. E. *Nano Lett.* **2007**, *7*, 1308–1313. (h) Wang, W.; Lu, X.; Zhang, T.; Zhang, G.; Jiang, W.; Li, X. *J. Am. Chem. Soc.* **2007**, *129*, 6702–6703. (i) Dong, A.; Tang, R.; Buhro, W. E. *J. Am. Chem. Soc.* **2007**, *129*, 12254–12262. (j) Blackman, B.; Battaglia, D. M.; Mishima, T. D.; Johnson, M. B.; Peng, X. *Chem. Mater.* **2007**, *19*, 3815–3821. (k) Robinson, R. D.; Sadtler, B.; Demchenko, D. O.; Erdonmez, C. K.; Wang, L. W.; Alivisatos, A. P. *Science* **2007**, *317*, 355–358. (l) Carbone, L.; et al. *Nano Lett.* **2007**, *7*, 2942–2950. (m) Teranishi, T.; Saruyama, M.; Kanehara, M. *Nanoscale* **2009**, *1*, 225–228. (n) McDaniel, H.; Zuo, J. M.; Shim, M. *J. Am. Chem. Soc.* **2010**, *132*, 3286–3288.

(9) Casavola, M.; Grillo, V.; Carlino, E.; Giannini, C.; Gozzo, F.; Pinel, E. F.; Garcia, M. A.; Manna, L.; Cingolani, R.; Cozzoli, P. D. *Nano Lett.* **2007**, *7*, 1386–1395.

(10) (a) Kolasinski, K. W. *Curr. Opin. Solid State Mater. Sci.* **2006**, *10*, 182–191. (b) Kuno, M. *Phys. Chem. Chem. Phys.* **2008**, *10*, 620–639.

(11) (a) Han, W.; Yi, L.; Zhao, N.; Tang, A.; Gao, M.; Tang, Z. *J. Am. Chem. Soc.* **2008**, *130*, 13152–13161. (b) Choi, S. H.; Kim, E. G.; Hyeon, T. *J. Am. Chem. Soc.* **2006**, *128*, 2520–2521.

(12) Connor, S. T.; Hsu, C. M.; Weil, B. D.; Aloni, S.; Cui, Y. *J. Am. Chem. Soc.* **2009**, *131*, 4962–4966.

(13) Du, W. M.; Qian, X. F.; Yin, J.; Gong, Q. *Chem.—Eur. J.* **2008**, *13*, 8840–8846.

(14) (a) Yoshino, K.; Ikari, T.; Shirakata, S.; Miyake, H.; Hiramatsu, K. *Appl. Phys. Lett.* **2001**, *78*, 742–744. (b) Pan, D. C.; An, L. J.; Sun, Z. M.; Hou, W.; Yang, Y.; Yang, Z. Z.; Lu, Y. F. *J. Am. Chem. Soc.* **2008**, *130*, 5620–5621. (c) Panthani, M. G.; Akhavan, V.; Goodfellow, B.; Schmidtke, J. P.; Dunn, L.; Dodabalapur, A.; Barbara, P. F.; Korgel, B. A. *J. Am. Chem. Soc.* **2008**, *130*, 16770–16777.

(15) (a) Tang, J.; Hinds, S.; Kelley, S. O.; Sargent, E. H. *Chem. Mater.* **2008**, *20*, 6906–6910. (b) Guo, Q.; Ford, G. M.; Hillhouse, H. W.; Agrawal, R. *Nano Lett.* **2009**, *9*, 3060–3065.

Scheme 1. Synthetic Route for Preparing of Ag_2S-CdS-ZnS and Ag_2S-ZnS-CdS-ZnS Heterostructures

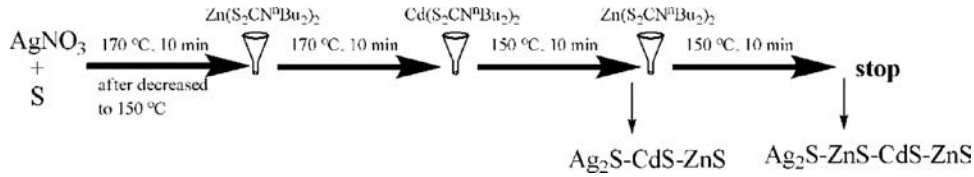

the novel catalyst and mediator for construction of heterostructures. As we well-known, Ag_2S is a kind of fast ion conductor and Ag cations in Ag_2S behave like a "fluid"; therefore, although Ag_2S is a stoichiometric compound, there are a lot of cation vacancies in Ag_2S NCs.[16] This unique feature would enable Ag_2S NCs potentially to be an excellent host mediator for fabrication of semiconductor heterostructures with special functions for various applications, especially in the photovoltaic field.

Here, we demonstrate that Ag_2S NCs are the bifunctional mediator acting as catalyst or source-host matrix for the preparation of semiconductor−semiconductor heterostructures such as acting as a catalyst for construction of Ag_2S-ZnS, Ag_2S-CdS, Ag_2S-CdS-ZnS, and Ag_2S-ZnS-CdS-ZnS and acting as a source-host matrix for fabrication of Ag_2S-$AgInS_2$, $AgInS_2$-Ag_2S-$AgInS_2$, and $AgInS_2$.

Experimental Section

Materials. $AgNO_3$, sulfur powder, *n*-heptane, $CHCl_3$, $AgNO_3$, $ZnSO_4$, $CdSO_4$, $InCl_3$, NaOH, *n*-dibutylamine, CS_2, methanol, and ethanol employed in this research are commercially available analytical-grade products. Octadecylamine (ODA, >98%) is purchased from Shanghai Chemical Factory (Shanghai, China). Dodecylamine were obtained from Aldrich (>98%). All reagents were used as received without further purification.

Synthesis of M(dbdc)$_x$ (M = Zn, Cd, In, Ag, dbdc = $S_2CN^nBu_2$, x = 1, 2, 3) Precursor. The synthesis of these precursors followed the method in previous works.[14b,17] In the synthesis of the Zn(dbdc)$_2$, NaOH (2.64 g) and *n*-dibutylamine (11 mL) were added to methanol (80 mL) in a bottle immersed in an ice water bath. Then CS_2 (3.96 mL) was added into the mixture dropwise. This yellow solution was mixed with aqueous solution of $ZnSO_4$ (80 mL, containing $ZnSO_4 \cdot 7H_2O$ 9.5 g) and stirred vigorously for at least 3 h. The product was separated by filtration, washed with water several times, and dried at room temperature. Using a similar route, the Ag(dbdc), Cd(dbdc)$_2$, and In(dbdc)$_3$ were prepared.

Synthesis of Ag_2S Nanocrystals. The synthesis of spherical silver sulfide nanocrystals was accomplished by direct reaction of $AgNO_3$ and S powder in octadecylamine as a solvent. Typically, octadecylamine (4.0 g) was heated to 170 °C at a rate of 8 °C min^{-1} in an opened round-bottom flask with bubbling N_2 and kept at this temperature for 20 min with stirring to get rid of water and other volatile impurities in the octadecylamine. Then $AgNO_3$ (25 mg) and S powder (29 mg) were added in turn. After the addition of S powder, the color of the reaction mixture changed from straw yellow to jet black, indicating the formation of Ag_2S nanocrystals. After further reaction for ∼10 min at 170 °C, the Ag_2S nanocrystals were precipitated using ethanol as a bad solvent and collected by centrifugation. After being washed by *n*-heptane and $CHCl_3$ several times, respectively, Ag_2S nanocrystals were used for further characterization and synthesis. Rodlike Ag_2S nanocrystals were synthesized with the same procedure but reacted at 95−130 °C.

Synthesis of Ag_2S-ZnS Heterostructures. Zn(dbdc)$_2$ (0.2−0.3 g) was dissolved in octadecylamine (or dodecylamine) (5−8 mL), and then $AgNO_3$ (3−10 mg) was added into the mixture. The reactor was heated to 150−260 °C at a rate of 8 °C min^{-1} and kept at this temperature for 7−60 min. The precipitate was collected by centrifugation, dispersed again in *n*-heptane and $CHCl_3$, and redeposited by the addition of ethanol for several cycles. In this case, Ag^+ reacted with Zn(dbdc)$_2$ forming Ag(dbdc), and the latter decomposed to form Ag_2S nanocrystals first at a temperature of about 120 °C; the ZnS species dissolved in and then grew out from Ag_2S nanocrystals when decomposition of Zn(dbdc)$_2$ occurred at about 140 °C.

Synthesis of Ag_2S-CdS Heterostructures. In a typical synthesis, silver sulfide nanocrystals were first prepared as described above. After the temperature of the above solution was decreased to 150 °C naturally, Cd(dbdc)$_2$ (12−24 mg) was then added under stirring and reacted for about 10−60 min at this temperature. The products experienced a similar rinsing process with that of Ag_2S-ZnS by *n*-heptane and $CHCl_3$. It is worth mentioning that it is difficult to clear up the remainder of the octadecylamine due to its high viscosity and the washing must be more than ten times.

For preparing Ag_2S-CdS heterostructures with longer CdS section, more Cd(dbdc)$_2$ is needed, for example, 60−120 mg of Cd(dbdc)$_2$. In this case, Cd(dbdc)$_2$ was added slowly with a small amount for each time, for example, 10 mg of Cd(dbdc)$_2$ was added every 6 min until all Cd(dbdc)$_2$ was added.

Synthesis of Ag_2S-CdS-ZnS, Ag_2S-ZnS-CdS-ZnS Heterostructures. The heterostructure with multisegments is prepared with a sequence-addition method. The preparation procedure is shown in Scheme 1. First, Ag_2S nanocrystals were synthesized by the method described in the synthesis of Ag_2S NCs. When the temperature fell to 150 °C naturally, Zn(dbdc)$_2$ (15 mg) was added in the above solution under stirring and reacted for about 10 min, then added Cd(dbdc)$_2$ (15 mg) and reacted for another 10 min, Ag_2S-CdS-ZnS heterostructures were formed. In above reaction solution another Zn(dbdc)$_2$ (15 mg) was added and reacted for about 10 min, Ag_2S-ZnS-CdS-ZnS heterostructures were produced. The products experienced similar rinsing process with that of Ag_2S-CdS by *n*-heptane and $CHCl_3$.

Synthesis of Ag_2S-$AgInS_2$ Heterostructure Nanocrystals. Silver sulfide nanocrystals were prepared at 170 °C as described above, and then the temperature was decreased to 150 °C naturally, and 10−55 mg of In(dbdc)$_3$ (2.2−12.1 mg/mL) was directly added into the above reaction solution under stirring and reacted for about 10 min at 150 °C. The products were washed by *n*-heptane and $CHCl_3$ more than 10 times.

Synthesis of Rodlike Ag_2S-$AgInS_2$, $AgInS_2$-Ag_2S-$AgInS_2$ Heterostructures. In a typical synthesis, rodlike silver sulfide nanocrystals were prepared as described above at 120 °C first. And then after decreasing the temperature to 150 °C, In(dbdc)$_3$ was added under stirring and reacted for about 10 min at this temperature, and rodlike Ag_2S-$AgInS_2$ heterostructures were obtained. Furthermore, $AgInS_2$-Ag_2S-$AgInS_2$ heterostructures were prepared at 170 °C using a similar route. The products experienced a rinsing process similar to that of Ag_2S-CdS by *n*-heptane and $CHCl_3$.

Synthesis of $AgInS_2$ Nanorods. Silver sulfide nanocrystals (0.07 mmol) were prepared with 25 mg of $AgNO_3$ and 29 mg of S at

(16) (a) Allex, R.; Moore, W. J. *J. Am. Chem. Soc.* **1959**, *63*, 223–226. (b) Lim, W. P.; Zhang, Z.; Low, H. Y.; Chin, W. S. *Angew. Chem., Int. Ed.* **2004**, *43*, 5685–5689. (c) Ivanov-Shitz, A. K. *Crystallogr. Rep.* **2007**, *52*, 302–315.
(17) Kemmler, M.; Lazell, M.; Obrin, P.; Otway, D. J.; Park, J. H.; Walsh, J. R. *J. Mater. Sci. Mater. Electron.* **2002**, *13*, 531–535.

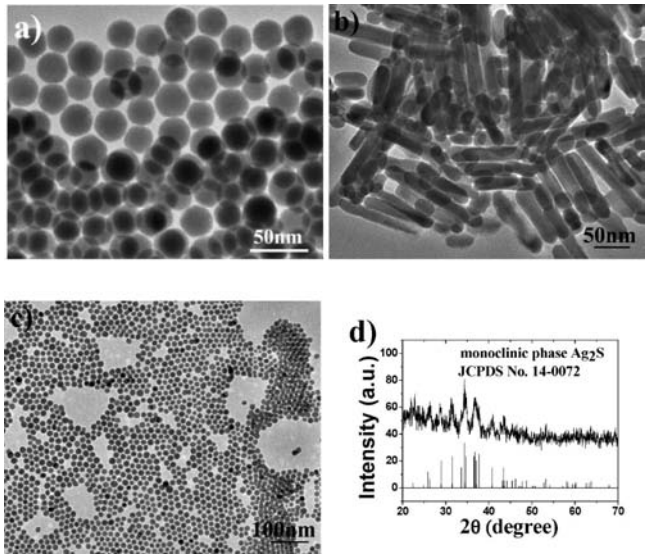

Figure 1. TEM images of Ag_2S samples obtained by the reaction between $AgNO_3$ and S in octadecylamine. (a) 170 °C, (b) 130 °C, and (c) 85 °C. (d) XRD pattern of Ag_2S nanocrystals with standard value for comparison.

170 °C without separating and purifying; after the temperature fell to 150 °C, 10 mg of $In(dbdc)_3$ was added and reacted for 6 min, and then another 10 mg of $In(dbdc)_3$ was added every 6 min until 100 mg of $In(dbdc)_3$ was added (the total $In(dbdc)_3$ is 0.14 mmol). The products were collected and washed using the same procedure as for Ag_2S-CdS.

Tracing the Growth Process of Ag_2S-ZnS Heterostructure. In dodecylamine (6 mL), 3 mL of Ag_2S nanocrystals colloid solution in $CHCl_3$ (containing Ag_2S nanocrystals about 0.02 mmol with a diameter of about 15 nm) was added. Then the system was heated to 150 °C with bubbling N_2, and the flask was kept open for 30 min to get rid of $CHCl_3$. After it was cooled to room temperature, 80 mg of $Zn(dbdc)_2$ was added, the reaction system was heated at a rate of 8 °C/min to 260 °C and samples were extracted in this heating process for further analyses.

Characterization. The X-ray powder diffraction patterns were recorded on an X'Pert diffractometer (Panalytical) with CuKα radiation ($\lambda = 1.54060$ Å) at 45 kV and 40 mA. Accumulation time for each sample was 20 min. Scanning electron microscopy (SEM) images were obtained using a Hitachi S-4800II field emission scanning electron microscope operated at 5 kV. High-resolution transmission electron microscopy (HRTEM) and energy-dispersive X-ray spectra (EDS) were performed on a JEOL-2100 microscope with an accelerating voltage of 200 kV. Transmission electron microscopy (TEM) samples were prepared by drop-casting dispersion onto copper grids covered by carbon film. Fourier transform (FFT) algorithms were performed using free software, *DigitalMicrograph*. Crystal structure model were simulated using the software *Diamond*.

Results and Discussion

Ag_2S Nanocrystals. Octadecylamine is used as a solvent and capping agent in the preparation of Ag_2S NCs. Its high boiling point (~349 °C) meets the requirement for subsequent preparations. The Ag_2S NCs were synthesized via a reaction between $AgNO_3$ and S powder in octadecylamine.

The size and shape of Ag_2S NCs are very sensitive to the reaction temperature and the dosage of $AgNO_3$ and S powder.[18] Spherical Ag_2S NCs were obtained (Figure 1a,c) when the temperature is higher than 160 °C or lower than 90 °C, but the former one, compared with the latter one, exhibits a large size and broader size distribution, whereas elongated Ag_2S nanocrystals (Figure 1b) were obtained at a middle temperature (95−130 °C). This is reasonable that at low temperature, the viscosity of octadecylamine solvent is high, and the diffusion rate of reactants is very low. The as-formed Ag_2S nuclei is capped tightly by octadecylamine, and it is of benefit for formation of spherical Ag_2S nanoparticles. When the temperature is increased to 95−130 °C, the viscosity of octadecylamine decreases, and the diffusion rate of the reactants increases and the capping agent partially desorbs from some faces of Ag_2S nuclei. All of these are of benefit for anisotropic growth to form elongated Ag_2S nanocrystals, which is consistent with the model reported by Peng's group.[19] After the temperature is increased to >160 °C, the reaction rate increases and the interaction between octadecylamine and Ag_2S is weaken; at same time, the second nucleation increases, which is of benefit for isotropic growth and a broad size distribution of Ag_2S.

The crystal structure of Ag_2S nanocrystals was analyzed by X-ray diffraction (XRD). The result shown in Figure 1d demonstrates that the nanoparticles are crystallized primitive monoclinic phase Ag_2S with lattice constants $a = 4.229$ Å, $b = 6.931$ Å, and $c = 7.862$ Å (JCPDS No. 14-0072). The high resolution transmission electron microscopy image (HRTEM) shows the single crystal nature of individual particles with near-spherical shape (Figure SI-1, Supporting Information). These Ag_2S NCs are directly used in the consequent preparation without further separation and purification. Ag_2S NCs are selected as a host matrix for construction of the semiconductor heterostructure as Ag^+ has very high mobility as if they are in a fluidic state in the S sublattice, as indicated by its unusually high ionic conductivity.[16]

Ag_2S NCs as Catalyst. The pre-experiments showed that the decomposition temperature of Ag(dbdc) (~120 °C) in organoamine is lower than that of $Zn(dbdc)_2$ (~140 °C). So, we designed a colloidal system composed of $AgNO_3$, $Zn(dbdc)_2$, and dodecylamine, in which Ag^+ reacts with $Zn(dbdc)_2$ to form Ag(dbdc) first, then the latter one decomposes earlier than $Zn(dbdc)_2$ to form Ag_2S NCs catalyst. In this method, the growth of Ag_2S NCs and ZnS nanowires (NWs) are self-regulated with the reaction time in one pot.

Figure 2a,b shows the SEM and TEM images of representative hexagonal phase ZnS NWs grown on Ag_2S NCs. The SEM image in Figure 2a reveals that the ZnS NWs are several micrometers long with a diameter of about 20 nm. At the end of the nanowire, a dark nanoparticle can be clearly seen (Figure 2b). The composition of the nanoparticle and the NW were determined by EDS recorded on the tip nanoparticle and the wire body, respectively (Figure SI-2, see Supporting Information). At least 10 tip nanoparticles and wires bodies were recorded and all give similar element components to prove that the tip nanoparticle is Ag_2S and the wire is ZnS. The phase structure of ZnS NWs was characterized by X-ray powder diffraction (XRD) shown in Figure 2c-A. The diffraction pattern matches well to hexagonal ZnS (JCPDS No. 80-0007), the high-temperature polymorph. The peaks between 30−45° attributed to Ag_2S are very weak because of its tiny quantity compared to ZnS.

Further HRTEM studies were carried out to obtain detailed information on the orientation relationship between Ag_2S NCs

(18) Wang, D. S.; Hao, C. H.; Zheng, W.; Peng, Q.; Wang, T. H.; Liao, Z. M.; Yu, D. P.; Li, Y. D. *Adv. Mater.* **2008**, *20*, 2628–3632.

(19) (a) Peng, Z. A.; Peng, X. G. *J. Am. Chem. Soc.* **2002**, *124*, 3343–3353. (b) Peng, X. G. *Chem.—Eur. J.* **2002**, *8*, 335–339. (c) Peng, X. G. *Adv. Mater.* **2003**, *15*, 459–463.

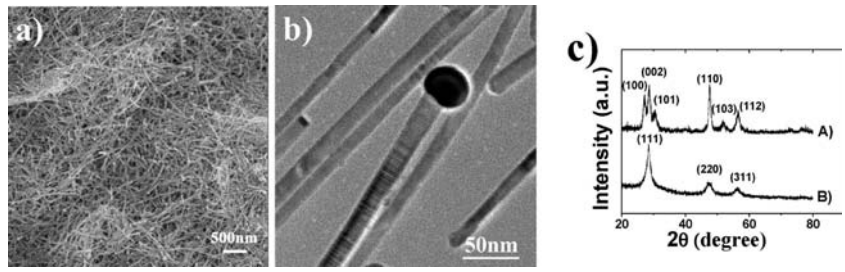

Figure 2. (a) SEM and (b) TEM images of typical synthesized Ag_2S-ZnS NWs heterostructures; (c) XRD patterns of (A) the Ag_2S-ZnS NWs heterostructures and (B) ZnS prepared without Ag_2S.

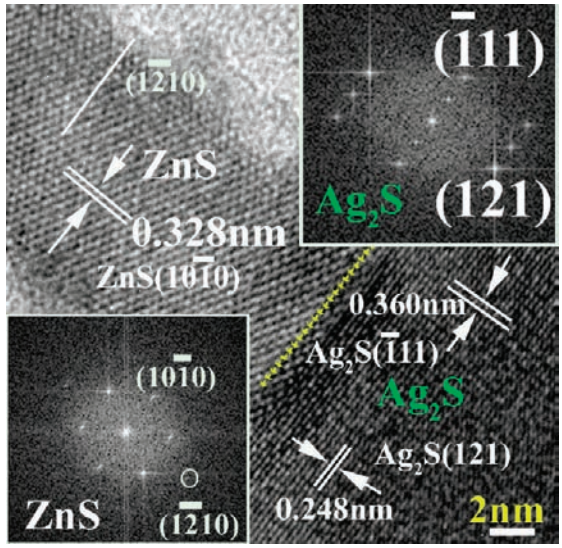

Figure 3. HRTEM image showing the heteroepitaxial growth of a hexagonal ZnS nanowire on an Ag_2S nanocrystal between $(1\bar{2}10)_{ZnS}$ and $(121)_{Ag2S}$. The insets: the corresponding Fourier transform (FFT) images from the Ag_2S area and the ZnS area.

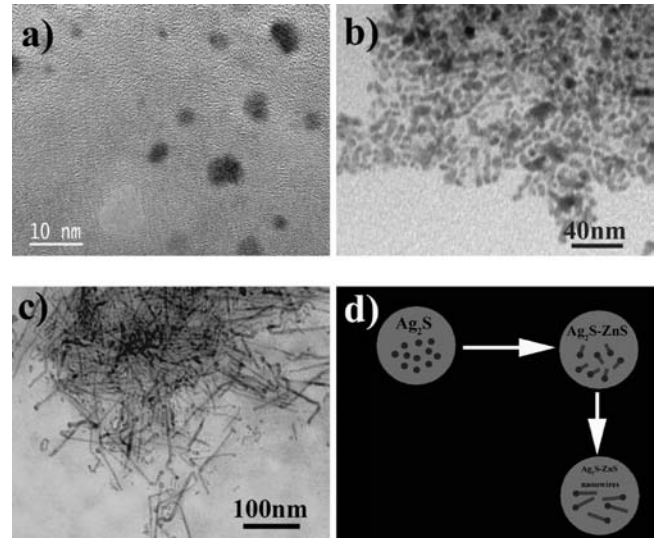

Figure 4. The growth process for the Ag_2S-ZnS NWs heterostructures at various stages as the temperature increases. TEM images of (a) the Ag_2S NCs formed when the system was heated to 130 °C, (b) the shorter ZnS nanorods grown on the Ag_2S NCs when heated to 150 °C, (c) the elongated ZnS NWs with Ag_2S NCs "head" were formed when further heated to 170 °C. (d) A schematic diagram of the heteroepitaxial growth process of ZnS NWs on Ag_2S NCs.

and ZnS NWs. The Ag_2S-ZnS interface and the corresponding FFT images are shown in Figure 3. It can be observed the interface is composed of the (121) plane of Ag_2S and the $(1\bar{2}10)$ plane of ZnS, and the preferential growth of ZnS NWs is along the direction of the $(1\bar{2}10)$ plane. A straightforward relationship of plane epitaxy can be proposed for the ZnS $(1\bar{2}10)$ and Ag_2S (121) plane. However, there is a large lattice mismatch (8.9%) between $(10\bar{1}0)_{ZnS}$ and $(\bar{1}11)_{Ag2S}$. The misfit-induced interfacial strain may be accommodated by the local curving near-interface junction or compensated by a decrease in the total surface energy due to solvent or surfactant binding.[2] Although the formation of the heterointerface with a large lattice mismatch seems to be explained by the coincidence site lattice model,[4e] we think that it is more likely to relate to the catalyst-assisted growth in solution and it will be further discussed later.

The synthesis method reported here is highly flexible; the diameter and length of ZnS NWs can be adjusted by the experiment parameters. Both the length and the diameter of ZnS NWs increase with the amount of $Zn(dbdc)_2$, while they decrease with an increase in the amount of $AgNO_3$. It is clear that the precursor $Zn(dbdc)_2$ and $AgNO_3$ play different roles; increasing the amount of $Zn(dbdc)_2$ will provide more Zn and S source for the growth of ZnS NWs, whereas increasing the amount of $AgNO_3$ will increase the numbers of Ag_2S NCs; therefore, decreasing the amount of ZnS dissolved in each Ag_2S NCs leads to a decrease in the length and the diameter of ZnS NWs.

In order to get an insight into the formation process of hexagonal ZnS NWs, an aliquot (~0.5 mL) of the reaction mixture was taken out the different reaction stages for TEM or EDS analyses. From the TEM images (Figure 4), we can see that nanoparticles are formed first at the beginning of the reaction (Figure 4a). EDS analysis recorded on one nanoparticle gives a composition of $Ag_{2.0}S_{1.2}$ (Figure SI-3, Supporting Information). The ZnS nanorods and longer NWs on Ag_2S nanoparticles are formed later (Figure 4b,c). The heterostructural boundary of the short nanorods (Figure 4b) can be clearly seen in the HRTEM image (Figure SI-4, Supporting Information). As mentioned above, the decomposition temperature of Ag(dbdc) (about 120 °C) is lower than that of $Zn(dbdc)_2$ (about 140 °C) with the assistance of aliphatic amine.[20] So, it is reasonable that Ag_2S nanoparticles are first formed and then ZnS species appear later when the reaction mixture is heated.

Ag_2S plays an important role for the subsequent growth (shape and phase) of ZnS. In the absence of Ag_2S, cubic ZnS NCs were obtained (Figure 2c-B, Figure SI-5, Supporting Information) instead of hexagonal ZnS NWs. Using other metal sulfides such as CuS, CdS, Bi_2S_3, and In_2S_3 instead of Ag_2S, a metal sulfide heterostructure cannot be formed; rather, cubic ZnS NCs and the corresponding metal sulfide are formed instead, which proves the unique role of Ag_2S NCs for the growth of ZnS NWs.

(20) Li, L. S.; Pradhan, N.; Wang, Y. J.; Peng, X. G. *Nano Lett.* **2004**, *4*, 2261–2264.

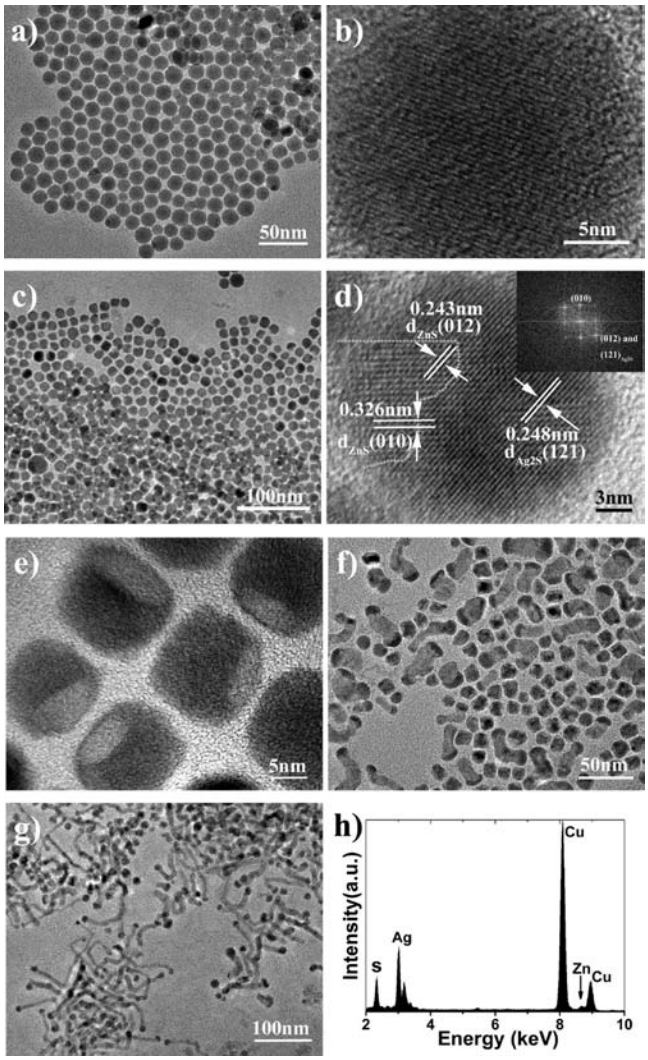

Figure 5. The growth process of ZnS nanowires on Ag_2S nanocrystals. (a, b) TEM images of samples extracted at 110 °C, (c−e) at 130 °C, (f) at 150 °C, and (g) at 170 °C. (h) EDS spectrum of the cubic nanoparticles extracted at 130 °C showing the existence of Ag, Zn, and S.

For clearly showing the feature of the catalytic growth of the heterostructures, the morphological evolution process of ZnS grown on Ag_2S nanoparticles was inspected. Ag_2S nanoparticles with diameters of 15 nm are first prepared via the reaction between $AgNO_3$ and S powder at 90 °C; after the system is cooled down to room temperature, $Zn(dbdc)_2$ are added. The reaction system is heated to 260 °C at a rate of 8 °C/min, and the reaction is traced over time.

The initial Ag_2S nanocrystals are nearly monodispersed nanospheres with an average diameter of 15 nm. HRTEM images show no other phase in these Ag_2S nanocrystals (Figure 5a,b). No obvious change of Ag_2S NCs was observed until 110 °C; however, when the temperature was increased to 130 °C (Figure 5c), the spherical Ag_2S nanocrystals become cubic nanoparticles composed of Ag_2S-ZnS heterostructure with a distinguishable interface (Figure 5d). EDS results demonstrate that both Ag and Zn are present in each individual particle, further supporting the conclusion that Zn has incorporated into the Ag_2S matrix to form the mixed-crystalline structure (Figure 5h). Some Janus-type heterostructure particles can also be observed at this reaction stage. With the temperature further

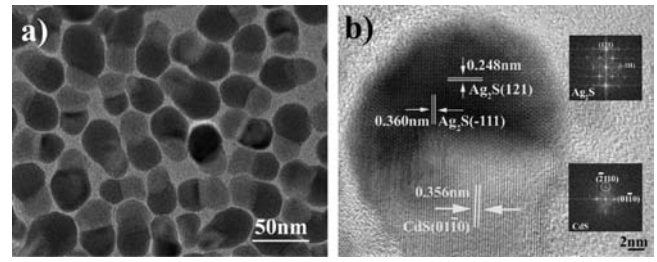

Figure 6. TEM images of (a) Ag_2S-CdS, (b) the corresponding interface orientation relationships.

increasing, ZnS grows into a 1D nanostructure with a hetero-interface between Ag_2S and ZnS (Figure 5f,g).

In this growth mode, the Ag_2S nanoparticle acts as a catalyst and Zn ions dissolve in Ag_2S and occupy Ag vacancy sites originated from the fluidic nature of the silver in Ag_2S. When the Zn concentration increases, ZnS clusters begin to aggregate to form ZnS phase. In order to reduce the high interfacial energy, the ZnS is pushed out from the silver sulfide "embryo" and starts to locate on a suitable plane of the Ag_2S nanoparticle with the smallest crystal-lattice mismatch. Consequently, Janus-type particles are formed, and ZnS NWs are grown out from the interface as the reaction proceeds.

Using Ag_2S NCs as a catalyst, Ag_2S-CdS heterostructures can also be constructed in octadecylamine with high yield. TEM and HRTEM images of Ag_2S-CdS are shown in Figure 6. From the HRTEM, we can see the CdS epitaxially attaches to the (121) plane of the Ag_2S section through its $(\bar{2}110)$ plane, meaning that the grain boundary is composed of $(\bar{2}110)_{CdS}$ and $(121)_{Ag2S}$. The interface orientation relationships between Ag_2S and CdS are $(\bar{1}11)_{Ag2S}$ // $(01\bar{1}0)_{CdS}$ (Figure 6b). The lattice mismatches along this direction are 3.7%. The length of CdS segment can be easily tuned by the amount of the precursor $Cd(dbdc)_2$. Figure 7 shows Ag_2S-CdS heterostructures with different lengths of CdS segment and their length distribution.

In addition to dimer heterostructures, the trimer and tetramer semiconductor heterostructures can also be constructed by this route through a sequence-addition method shown in Scheme 1.

The TEM images of Ag_2S-CdS-ZnS and Ag_2S-ZnS-CdS-ZnS are shown in Figure 8. A clear junction can be distinguished in the TEM images owing to the different contrast and diameter. EDS is used to examine the local atomic composition of the heterostructures. The results show that the trimer (Figure 8a,b) and tetramer (Figure 8c) heterostructures are composed of Ag_2S-CdS-ZnS and Ag_2S-ZnS-CdS-ZnS, respectively. It is valuable to note the arrangement order of ZnS and CdS segments in the trimer and tetramer. If the growth of the heterostructure follows a "seeded growth model", then CdS added late should grow on the tip of the ZnS segment in the trimer to generate Ag_2S-ZnS-CdS heterostructures. The arrangement order of the ZnS and CdS segment in trimer provided further evidence that the growth of the heterostructures follows a "catalyst-assisted growth model" and Ag_2S NCs act as a catalyst for growth of the heterostructures.

As shown in Figure SI-6 (see Supporting Information), the interfaces are composed of $(1\bar{2}10)_{ZnS}$ and $(\bar{2}110)_{CdS}$; $(\bar{2}110)_{CdS}$ and $(121)_{Ag2S}$ from which we can see that $(1\bar{2}10)_{ZnS}$ and $(121)_{Ag2S}$ are the same as the original interface in Ag_2S-ZnS. It clearly shows that the CdS segment grows between two interfacial facets in the Ag_2S-ZnS heterostructure, which provides further evidence for catalyst-assisted growth. The interface orientation relationships between ZnS and CdS are $(10\bar{1}0)_{ZnS}$ // $(01\bar{1}0)_{CdS}$

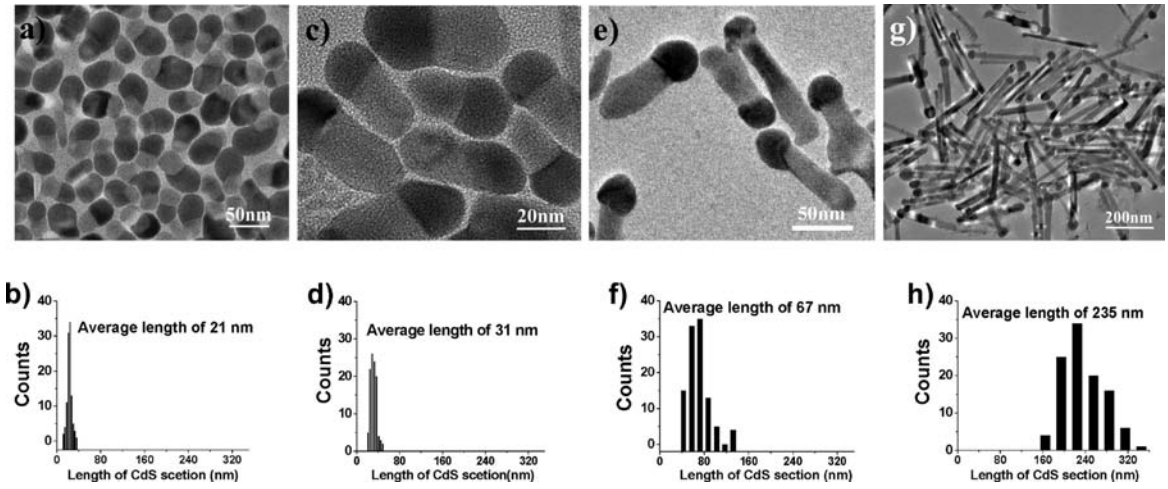

Figure 7. (a, c, e, g) TEM images of Ag_2S-CdS heterostructures, which show that the length of CdS segment increases with the amount of $Cd(dbdc)_2$: (a) 12 mg, (c) 24 mg, (e) 60 mg, and (g) 124 mg, and (b, d, f, h) the length distribution of CdS segment corresponding to the (a), (c), (e), (g) TEM images, respectively.

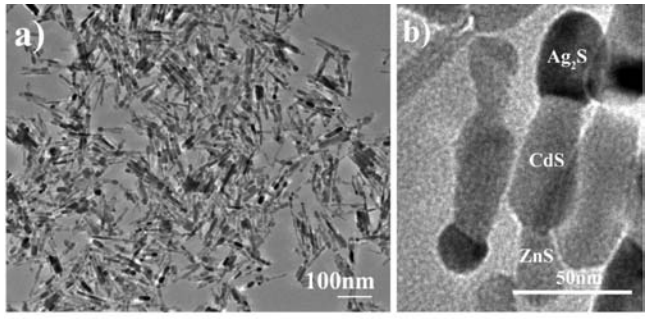

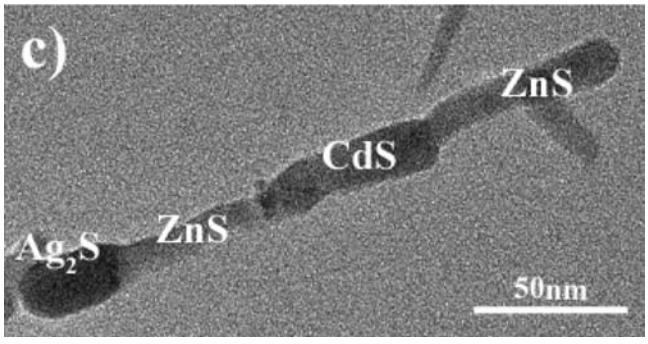

Figure 8. TEM images of (a, b) Ag_2S-CdS-ZnS and (c) Ag_2S-ZnS-CdS-ZnS heterostructures obtained by consequent addition of the corresponding precursors.

and $(0001)_{ZnS}$ // $(0001)_{CdS}$ (Figure SI-6, see Supporting Information). The lattice mismatches of these two groups of planes are quite large, 8.3% and 7.4%, respectively, which induces a shrink of the trimer at the interface forming a lotus rootlike morphology to reduce high interfacial energy, but the heterojunctions still can be formed via catalytic growth.

Ag_2S NCs as Resource-Host. As we know, I−III−VI_2 compound is a kind of important ternary semiconductor and is a promising material for photovoltaic applications. The construction of I−III−VI_2 ternary semiconductor heterostructures is an attractive front object for creating novel function materials.

As mentioned in the experimental section, Ag_2S-$AgInS_2$ heterostructure NCs were synthesized by a similar method, but in this case, Ag_2S NCs act as a source-host instead of a catalyst. In the absence of Ag_2S NCs, $In(dbdc)_3$ does not decompose to

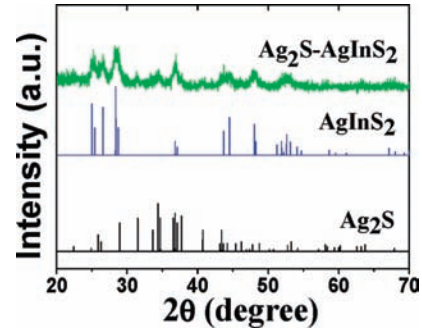

Figure 9. XRD pattern of as-prepared Ag_2S-$AgInS_2$ heterostructure nanocrystals. Ag_2S standard data from JCPDS No. 14-0072 and $AgInS_2$ standard data from JCPDS No. 25-1328 are also shown for comparison.

form In_2S_3 even at 280 °C, which is important for avoiding the self-nucleation of In_2S_3. On the basis of these, $In(dbdc)_3$ was adopted as a precursor, and the solid powder $In(dbdc)_3$ was directly added into a hot octadecylamine containing Ag_2S NCs to prepare Ag_2S-$AgInS_2$ heterostructures.

The XRD pattern of the Ag_2S-$AgInS_2$ heterostructure nanocrystals (Figure 9) clearly shows that the primitive monoclinic phase of Ag_2S coexists with the primitive orthorhombic phase of $AgInS_2$ with a lattice constant $a = 7.001$ Å, $b = 8.278$ Å, and $c = 6.698$ Å (JCPDS No. 25-1328). The orthorhombic phase is a metastable state of $AgInS_2$, which usually forms at a temperature higher than 620 °C, while the tetragonal phase appears below 620 °C.[21] The formation of metastable orthorhombic $AgInS_2$ in such a lower temperature (150 °C) could be attributed to the change of the chemical growth environment such as solvent, surfactants, and mediator, which results in a temporary phase reversion.[22]

Typical TEM image of the Ag_2S-$AgInS_2$ heterostructure nanocrystal is shown in Figure 10a, which reveals that the obtained nanocrystal is composed of a hemispherical "head" and a rodlike "stick", forming a matchstick-like morphology.

(21) (a) Roth, R. S.; Parker, H. S.; Brower, W. S. *Mater. Res. Bull.* **1973**, *8*, 333–338. (b) Krustok, J.; Raudoja, J.; Krunks, M.; Mandar, H.; Collan, H. *J. Appl. Phys.* **2000**, *88*, 205–209.
(22) (a) Tian, L.; Elim, H. I.; Ji, W.; Vittal, J. J. *Chem. Commun.* **2006**, 4276–4278. (b) Wang, D. S.; Zheng, W.; Hao, C. H.; Peng, Q.; Li, Y. D. *Chem. Commun.* **2008**, 2556–2558.

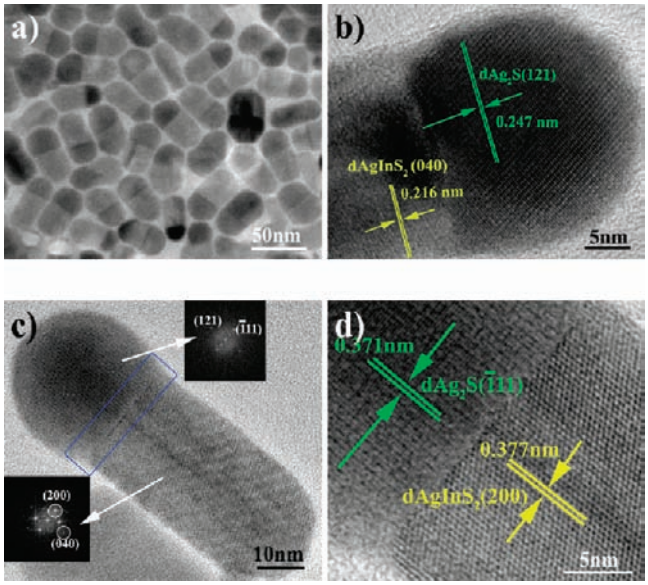

Figure 10. (a) Typical TEM image of the obtained Ag_2S-$AgInS_2$ heterostructure nanocrystals with a $In(dbdc)_3$ concentration of 4.8 mg/mL (22 mg of $In(dbdc)_3$). (b) HRTEM image shows the lattice planes of grain boundary. (c) TEM image of a typical Ag_2S-$AgInS_2$ heterostructure nanocrystal. The insets show the corresponding FFT, which further gives the detailed structure of the heterojunction. (d) HRTEM image from the area circled by a blue line in (c).

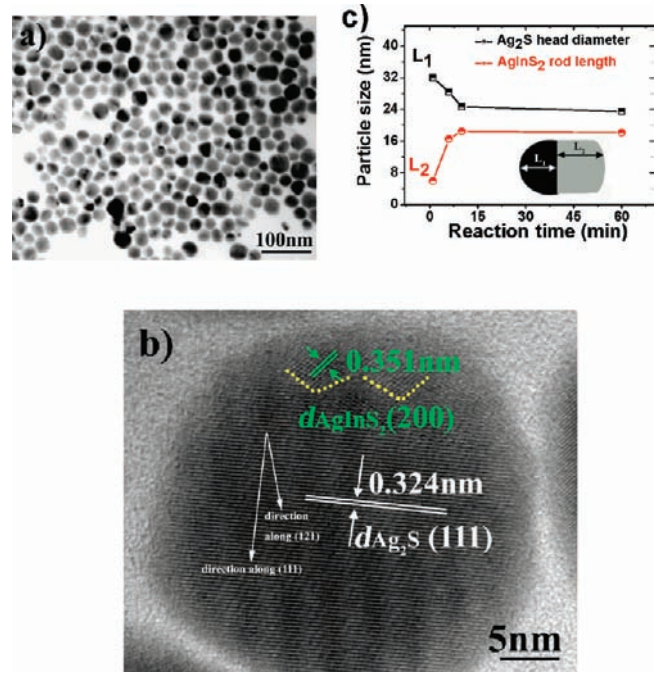

Figure 11. (a, b) TEM images of the Ag_2S-$AgInS_2$ sample extracted after the addition of 15 mg of $In(dbdc)_3$ solid (3.3 mg/mL) and reaction for 1 min. (c) The size evolution of the heterostructure nanocrystals and Ag_2S NCs.

The junction area is very narrow and no gradual transition layer is observed. EDS analyses are conducted on the corresponding microareas of head and stick (Figure SI-7, Supporting Information). The results confirm the head is Ag_2S and the stick is $AgInS_2$.

HRTEM investigations are performed to determine the detailed structure of the heterojunction between Ag_2S and the $AgInS_2$. The HRTEM image in Figure 10b shows that the interface is composed of $(121)_{Ag2S}$ and $(040)_{AgInS2}$. The HRTEM images in Figure 10c,d reveal that the $(\bar{1}11)_{Ag2S}$ and $(200)_{AgInS2}$ are perpendicular to the interface. On the basis of these analyses, an atomic packing model is proposed in Figure SI-8, Supporting Information to depict the formation of heterojunction between the orthorhombic phase $AgInS_2$ and the monoclinic phase Ag_2S (see Supporting Information). The interface-orientation relationship between the Ag_2S and $AgInS_2$ is $(\bar{1}11)_{Ag2S}$ // $(200)_{AgInS2}$ with a lattice mismatch 1.6%. The relatively smaller lattice mismatch enables the inward growth of orthorhombic phase $AgInS_2$ in the monoclinic phase Ag_2S with a flat interface structure. The synthesis of Ag_2S-$AgInS_2$ heterostructure developed here is quite facile. It can be conducted even under open air and it is not necessary to protect with an inert atmosphere. Also, the formation of Ag_2S-$AgInS_2$ heterostructures is not sensitive to the surfactants such as oleic acid or organoamine.

The length of generated $AgInS_2$ can be approximately estimated from the consumed Ag_2S (Figure SI-9−11, Supporting Information). Considering the Ag species in $AgInS_2$ all comes from Ag_2S nanocrystals and the difference of Ag densities in Ag_2S and $AgInS_2$, the volume of $AgInS_2$ will enlarge 3.42 times than Ag_2S when Ag_2S is transferred to $AgInS_2$, which is similar to the experimental results.

To further understand the formation process of the heterostructures, the morphological evolution of the heterostructures is monitored by TEM. Representative images of samples at various reaction times are shown in Figure 11 and Figure SI-12 (Supporting Information). The initial near-spherical Ag_2S nanocrystals are nearly monodispersed. One minute later after the addition of $In(dbdc)_3$, $AgInS_2$ NCs have grown in Ag_2S NCs (about 5 nm) and formed a clear domain (Figure 11a,b), while the shape of the nanocrystal is still near-spherical. At same time, no isolated $AgInS_2$ crystalline is observed in the reaction solution. The corresponding interfaces are shown in Figure 11b and the interfacial relationship was analyzed (the deducing process is shown in Figure SI-13 (Supporting Information). At the beginning, the interface is composed of several different interfacial structures and appears as a sawtooth-like. After reaction for 6 min, heterostructure nanocrystals with a single and flat interfacial structure are formed (Figure SI-12a,b, Supporting Information). The interface with high energy will grow fast and diminish rapidly until vanishing finally. At the same time, the interface with a smaller lattice mismatch, namely, that with lower energy, will enlarge more quickly to form a single and flat interface finally.

The length of $AgInS_2$ in Ag_2S-$AgInS_2$ heterostructure NCs increases with the time until the reaction for 10 min (Figure SI-12c, Supporting Information), then it remains almost constant for another 50 min because of the exhaustion of the reaction species (In cations) (Figure SI-12d, Supporting Information). The evolution of length with respect to time is shown in Figure 11c, which shows that the Ag_2S segment becomes shorter and the $AgInS_2$ becomes longer with reaction time. At the same time, the interfacial structure of Ag_2S-$AgInS_2$ remains flat and narrow, which means that no alloying process takes place for these Janus-type nanostructures in 60 min. The above results further confirm that Ag_2S acts as a source and a host for subsequent growth of $AgInS_2$.

The morphology of the Ag_2S-$AgInS_2$ heterostructures can be easy adjusted by Ag_2S NCs. Using spherical Ag_2S NCs as the source-host, the matchstick-like heterostructures are obtained, whereas rodlike heterostructures are formed when rodlike Ag_2S NCs are adopted as mediators. Figure 12a is the TEM image

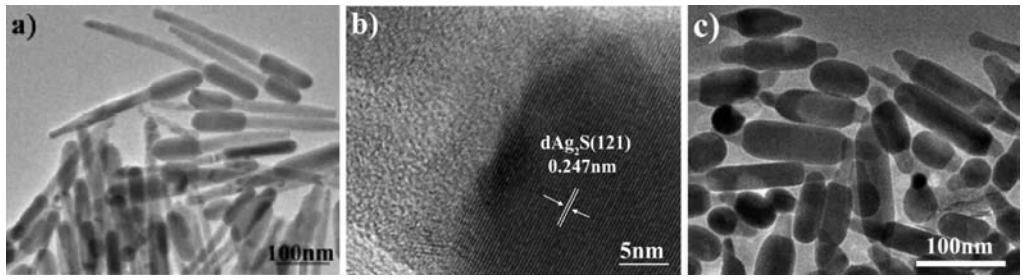

Figure 12. (a) TEM image of rodlike Ag_2S-$AgInS_2$ heterostructures with rodlike Ag_2S as source-host reacted at (a) 150 °C and (c) 170 °C, (b) HRTEM of the interface showing $AgInS_2$ grown on the (121) plane of Ag_2S.

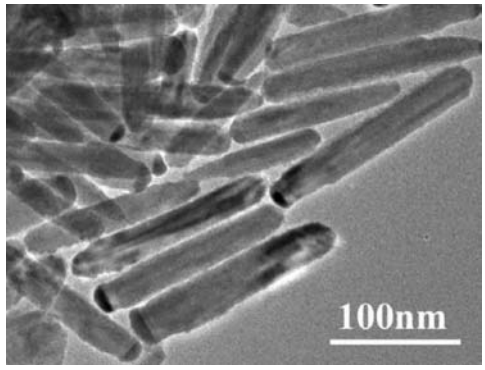

Figure 13. TEM image of the $AgInS_2$ nanorods with a small Ag_2S segment prepared with the addition of 100 mg of $In(dbdc)_3$ by a rate of 10 mg/6 min (the final concentration of $In(dbdc)_3$ is 22 mg/mL), which makes the concentration of $In(dbdc)_3$ at a lower level.

of the rodlike Ag_2S-$AgInS_2$ heterostructures. The $AgInS_2$ segment grows on one end of the Ag_2S rod. HRTEM observation shows that the $AgInS_2$ segment also grows on the (121) plane of Ag_2S (Figure 12b), which is the same as the case of spherical Ag_2S as the source-host. After the temperature is increased to 170 °C, $AgInS_2$ nanorods grow on both ends of the Ag_2S rod, forming $AgInS_2$-Ag_2S-$AgInS_2$ trimer heterostructures, as shown in Figure 12c.

Similar to the case of Ag_2S-ZnS, the high mobility of Ag^+ promotes the generation of a lot of Ag^+ vacancies in Ag_2S NCs, which is believed to benefit the diffusion of In species into Ag_2S NCs to form $AgInS_2$ species. The as-formed $AgInS_2$ species aggregate and form $AgInS_2$ phase as the concentration of $AgInS_2$ species increases. At the beginning, the interfacial structure is not single. As the reaction proceeds, the interface with a smaller lattice mismatch develops preferentially, while others decrease rapidly to reduce interfacial energy. Finally, a single and flat interfacial structure is formed with the smallest lattice mismatch. The (121) plane of Ag_2S prepared in octadecylamine would be such a platform for the location of $AgInS_2$. After the formation of a stable heterointerface, $AgInS_2$ inwardly grows along the direction of the interface of the Ag_2S-$AgInS_2$ heterojunction in Ag_2S NCs until all Ag_2S is exhausted, if the In cations are enough, to form single phase $AgInS_2$ nanocrystals (Figure 13). In this growth model, the length of $AgInS_2$ segment in Ag_2S-$AgInS_2$ heterostructures can be easily adjusted and controlled by adjusting the amount of $In(dcdb)_3$. This growth feature is different from the Cu−In sulfide nanocrystals reported by Hyeon et al.[11b] and Cui et al.[12] In these cases, the growth of heterostructures follows a "seeded growth model" to form Cu_2S-In_2S_3 or Cu_2S-$CuInS_2$ heterostructures. Also, it is different from that reported by Tang et al.,[11a] which followed a catalyst-assisted growth model to form Cu_2S−In_2S_3; at same time, the catalyst $Cu_{1.94}S$ underwent transformations in both crystalline structure and chemical composition (from monoclinic djurleite to hexagonal chalcocite during the formation of the heterostructure). The reason for this is not clear at the present time; it might be related to the crystal structure and the cation mobility of Cu_2S. Compared with the hexagonal phase Cu_2S, monoclinic $Cu_{1.94}S$ has high cation mobility and, therefore, has more cation vacancies, which is of benefit for a foreign cation dissolving. So, $Cu_{1.94}S$ is a good catalyst but Cu_2S is not and only acts as a seed. But $Cu_{1.94}S$ is not stable and is easily transform into Cu_2S, which prevents it from being used as a catalyst for the construction of trimer or tetramer of semiconductor heterostructures.

Summarizing the above results, the difference of two growth models is as follows: in the catalyst-assisted growth model, Zn^{2+} (or Cd^{2+}) dissolves in the Ag_2S NCs catalyst to form ZnS (or CdS) species, which does not consume Ag_2S at all. As ZnS or CdS species accumulate, they aggregate and form their own phase. In order to decrease the interfacial energy, they are pushed out from Ag_2S "embryo" to reduce the interface area and grow through epitaxial mode. At the same time, the interface with the smaller lattice mismatch preferentially develops, whereas in the source-host growth model, In^{3+} dissolves in Ag_2S and simultaneously reacts with Ag_2S to form $AgInS_2$ species, which consumes Ag_2S, although the consequent process including the phase isolation and growth of $AgInS_2$ NCs is similar to the catalyst-assisted growth model. Ag_2S NCs act not only as a catalyst providing a host to accommodate the foreign species, but also as one source for the subsequent formation of $AgInS_2$ (and also, the $AgInS_2$ NCs grow in Ag_2S via inward growing mode).

In addition, the Ag_2S-based heterostructures prepared here are stable at ambient conditions. As shown in Figure SI-14, the heterostructures synthesized do not have observable degradation after 4−20 months in solid state or on the carbon film of copper grids.

We believe that, through appropriate design, this kind of sulfide heterostructure can find further interesting applications ranging from nanoelectronic to optoelectronic, biomedical, photovoltaic, and catalytic. In order to apply in photovolatics and sensors field, it is needed to connect the ends of the heterostructures electrically for input and output, and therefore, a longer segment of the heterostructure is desirable. Although long nanowires/rods of ZnS, CdS, and $AgInS_2$ in the heterostructures prepared here have been achieved, the Ag_2S segment in Ag_2S-ZnS and Ag_2S-CdS heterostructures is slightly shorter and it needs improvement. In addition, further work we are planning to do is extending the spectrum of the semiconductor catalyst and developing a method for the hierarchical assembly of these nanoheterostructures with exquisite spatial control to

enable continued progress in this field to fabricate new and interesting nanosystems.

Conclusions

It was demonstrated that Ag_2S nanocrystal is a novel bifunctional semiconductor mediator for growth of semiconductor heterostructures in solution-phase. On the basis of its high Ag^+ ion mobility, Ag_2S nanocrystals not only exhibit excellent catalytic function for growth of metal sulfide (ZnS, CdS) heterostructures, but also can act as a source-host for the growth of ternary semiconductor heterostructures, for example, biphase Ag_2S-$AgInS_2$ and single phase $AgInS_2$ nanorods. In the latter case, Ag_2S exhibits both catalyst and source materials functions. The heterostructure morphology, including the length and diameter, can be adjusted and controlled easily by adjusting reaction conditions. HRTEM and FFTs results reveal that the single-crystalline semiconductors grow epitaxially from or inward in Ag_2S nanocrystals. The analysis of the orientation relationship of the interface reveals that the interfacial structure can be stable even if the lattice mismatch is quite large. Moreover, the method developed here also can be used to construct multisegments heterostructures, for example, Ag_2S-CdS-ZnS, $AgInS_2$-Ag_2S-$AgInS_2$, and Ag_2S-ZnS-CdS-ZnS. All these show that semiconductor Ag_2S nanocrystal is a new type of nanomediator acting as a catalyst or a source-host, which will be self-switched on the reaction system. The high mobility of the cations creates a lot of vacancies, which allows foreign cations to dissolve. It is quite different from the metal nanoparticle catalyst and opens a new avenue to develop new catalysts for construction of novel semiconductor heterostructures and devices with novel functions and properties.

Acknowledgment. Financial Support from National Major Basic Research Program (973 program 2007CB936302) and the National Natural Science Foundation of China under major project No. 90606005 is greatly appreciated.

Supporting Information Available: EDS analysis of the heterostructures, TEM and HRTEM images of Ag_2S, ZnS, Ag_2S-CdS-ZnS, the growth process of Ag_2S-$AgInS_2$, schematic model for the atomic arrangements of the epitaxial planes of $AgInS_2$ (200) and Ag_2S ($\bar{1}11$), calculation of the length of $AgInS_2$ segment from the reacted Ag_2S, filter treatment of HRTEM image shown in Figure 11b, and complete ref 8l. This material is available free of charge via the Internet at http://pubs.acs.org.

JA1090996